




# Light-weight and flexible Ni-doped CuO (Ni:CuO) thin films grown using the cost-effective SILAR method for future technological requests

R. Aydın<sup>1</sup>, A. Akkaya<sup>2,\*</sup> , and B. Şahin<sup>3</sup>

<sup>1</sup>Department of Physics, Faculty of Sciences, Selçuk University, Konya, Turkey

<sup>2</sup>Mucur Technical Vocational Schools, Tech. Prog. Department, Kırşehir Ahi Evran University, Kırşehir, Turkey

<sup>3</sup>Department of Physics, Faculty of Arts and Sciences, Mustafa Kemal University, Hatay, Turkey

Received: 13 July 2022

Accepted: 12 September 2022

Published online:  
23 September 2022

© The Author(s), under exclusive licence to Springer Science+Business Media, LLC, part of Springer Nature 2022

## ABSTRACT

Products based on nanostructured flexible thin films, which are anticipated to make their way into our lifetimes in the near future. Therefore, nanostructured metal-oxide thin-film materials grown on flexible substrates are anticipated to meet emerging technological requests. In this article, we present a promising light-weight and flexible thin-film material using un-doped and Ni-doped CuO samples. Ni:CuO flexible thin-film materials were fabricated by using the cost-effective SILAR method on cellulose acetate substrates and the effects of both Ni doping and bending on the change in electrical and optoelectronic performances were investigated. It is observed that Ni doping has a great impact on the main physical properties of flexible CuO samples. The optical bandgap value of the un-doped CuO film improves with increasing Ni ratio in the growth bath. Also, sheet resistance values of the un-doped and Ni:CuO samples are a little affected due to bending of samples for bending radius  $\sim 20$  mm. These flexible all solution-processed nanostructured CuO samples are promising candidates for use in future optoelectronic applications.

## 1 Introduction

Microdevices, such as pH sensors, gas sensors and printed electronics received significant attention in many fields, including health monitoring systems and low-cost wearable sensing electronics [1, 2]. In particular, devices made with doped metal-oxide materials (MOs), such as ZnO, CuO, NiO, SnO<sub>2</sub>, and TiO<sub>2</sub>, with semiconductor properties are extremely

important in this regard and have been the subject of much research [3–5]. MOs represent one of the important classes of functional materials in terms of their abundance for their practical use and added value opportunities for continuous quality/performance improvement. These MOs are one of the most common groups of compounds on earth, with a wide variety of chemical compositions, atomic structures, and crystalline shapes. Almost all known effects can

Address correspondence to E-mail: [abdullah.akkaya@ahievran.edu.tr](mailto:abdullah.akkaya@ahievran.edu.tr)

be observed in MOs, including superconductivity, thermoelectric effects, photoelectric effects, luminescence and magnetism. In addition, MOs have played a key role in the successful application of device technologies for many years due to their unique combination of redox chemistry, optics, electrical and semiconductor properties [6, 7]. This attractive class of materials can be fabricated economically on flex substrates [8]. Among these MOs, the prominent one is (CuO), also known as cupric oxide, due to its widespread availability, stability, low cost and ease of synthesis. CuO has an indirect optical narrow bandgap (of roughly 1.4 eV). It shows p-type conductivity with a big carrier concentration in the range of  $10^{17}$ – $10^{22}$  cm<sup>-3</sup> due to the excess of copper or oxygen vacancies in its structure. [2, 9–11].

Due to its excellent electrical, optical, chemical, and physical properties and its ability to be produced with this simple production technique, CuO films find various uses/applications in various gas sensors, optical devices, and the production of some semiconductor-based devices. Moreover, some of its physical properties can be rearranged by doping. Especially, different element ions such as Ni, Li, Ag, Co, Al, In, Zn, etc. into the metal-oxide lattice structure to improve the physical properties and to modify the band structures of films have been investigated.

CuO films on which the device will be built can be obtained using different methods (sputtering, electrochemical deposition, pyrolysis, chemical bath/spray deposition, and successive ionic layer adsorption and reaction (SILAR) [12–16]. Here, SILAR is the most preferred technique due to its own simple and low-cost nature [16–18]. Nowadays, there is a large interest in novel materials which allow for elevated efficiency electronic devices to be generated onto flexible substrates. These new generation flexible electronic materials open up a broad range of exciting novel implementations such as wearables with sensors that help monitor health condition, textiles, architecture, and light-weight energy harvesting materials [19, 20].

In addition to this easily accessible production technique, devices produced on flexible substrates are needed to meet the requirements of wearable devices and real-time monitoring systems. To optimize the integration of sensors or microdevices with monitoring systems and to build integrated systems, it is necessary to build these devices on flex substrates. Thus, built on flexible and transparent

substrates, some metal-oxide-based nanostructures have attracted significant attention considering their unique properties [21, 22]. Currently, several research groups have reported different types of sensors on electrical insulated and flexible substrates, such as polyimide (PI), polyethylene naphthalate (PEN), cellulose acetate (CA) and polyethylene terephthalate (PET) [2, 21, 23]. This semi-transparent and/or flexibility properties of CuO on flexible substrates facilitate future applications and integration with wearable systems and sensors [21, 22].

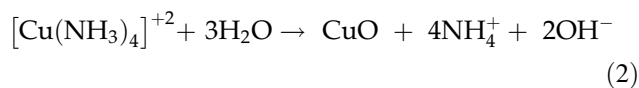
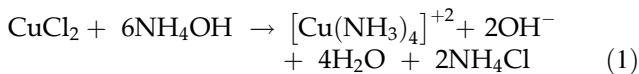
It is important to investigate the metal-oxide nanostructures and such as how the slightly doping process changes optoelectronic features and electrical conductivity are altered when the composition varies. In this article, un-doped CuO and Ni (1.0%, 2.0% and 4.0%)-doped CuO thin films were fabricated on flexible cellulose acetate (CA) substrates by using the SILAR technique. X-ray diffractometers (XRD), scanning electron microscopy (SEM), and atomic force microscopy (AFM) ensured information of the crystalline structure and surface morphology of the CuO samples. The optical characteristics of the samples were examined by ultraviolet–visible (UV–Vis) spectroscopy. The electrical properties of un-doped CuO and Ni-doped CuO films on a flexible substrate were characterized using sheet resistivity measurements for normal and bending conditions.

## 2 Experimental details

In the experiment, materials such as copper (II) chloride dehydrate ( $\text{Cl}_2\text{CuH}_4\text{O}_2$ ,  $\geq 99.0\%$ ), nickel (II) nitrate hexahydrate ( $\text{H}_{12}\text{N}_2\text{NiO}_{12}$ ,  $\geq 98.5$ ), ammonium hydroxide ( $\text{NH}_4\text{OH}$ ), sulfuric acid and acetone ( $\text{C}_3\text{H}_6\text{O}$ ) were used as source material without any purification to synthesize un-doped and Ni-doped CuO films. These chemicals, available from international commercial suppliers such as Merck Company and Sigma-Aldrich Company, are at analytical reagent grade. Distilled water and ammonium hydroxide were used as solvents.

Un-doped and  $\text{Cu}_{1-x}\text{Ni}_x\text{O}$  ( $x$ : 0.01, 0.02 and 0.04) films were synthesized on CA substrates using the SILAR procedure. The solution was prepared from 150 ml 0.1 M copper (II) chloride in distilled water and was stirred with a magnetic stirrer for 5 min at room temperature to obtain a stable solution.  $\text{NH}_4\text{OH}$  was added to assay the pH of the bath to about 10

and the solution was heated to about 75 °C. To obtain CuO film, the CA substrates were immersed in the reaction bath for 20 s and then in a cleaning bath (distilled water) for 20 s to remove weakly bound ions. A total of 35 SILAR cycles were performed to synthesize a homogeneous CuO film of the desired thickness. The schematic of the SILAR method to obtain the CuO film is presented in Fig. 1. Possible chemical reactions occurring during the SILAR deposition process of CuO film are given in Eqs. 1 and 2 [24]:



To investigate the effects of Ni (1.0%, 2.0% and 4.0%) doping element, Ni-doped CuO films were synthesized in the same way. The obtained films were labeled as un-doped CuO,  $\text{Cu}_{0.99}\text{Ni}_{0.01}\text{O}$ ,  $\text{Cu}_{0.98}\text{Ni}_{0.02}\text{O}$  and  $\text{Cu}_{0.96}\text{Ni}_{0.04}\text{O}$ .

A profilometer NanoMap 500LS 3D (AEP technology) was used to measure the thickness of the CuO and Ni-doped CuO films. A Bruker D8 Advance X-ray diffractometer (using  $\text{CuK}\alpha$   $\lambda = 0.1518$  nm radiation, 40 kV, 30 mA) ( $\text{CuK}\alpha 1$ ,  $\lambda = 1.5405$  Å, 45 kV, 40 mA) was used to examine the crystalline quality of all deposited CuO films. Surface properties along with elemental content were examined using an Evo Ls 10 (Carl Zeiss NTS, accelerating voltage;

18 kV) scanning electron microscopy (SEM) equipped with energy-dispersive X-ray spectroscopy (EDX, Detector; Bruker AXS, XFlash Detector 5010, analysis software; QUANTAX ESPRIT 1.9). An atomic force microscope (AFM) NT-MDT/Ntegra Solaris [Nova (Nova\_11147\_win32\_Release)] was used to examine the morphology and root mean square (RMS) distribution of grains. A Genesys 10S UV-Vis. spectrophotometer (Thermo Scientific, the spectral range from 190 to 1100 nm) was employed to measure the absorption of the spectra. A Keithley 6487 picoammeter/voltage source (Keithley Instruments, Cleveland, OH), was used to determine the sheet resistances of all deposited CuO films.

### 3 Results and discussion

#### 3.1 Morphological properties

The morphology of flexible un-doped and Ni-doped CuO films with different Ni doping ratios (1.0%, 2.0% and 4.0%) was studied using SEM. The SEM photographs of un-doped CuO and  $\text{Cu}_{1-x}\text{Ni}_x\text{O}$  ( $x$ : 0.01, 0.02 and 0.04) films are shown in Fig. 2. From the SEM photographs, it is seen that the surface morphologies of both un-doped and Ni-doped CuO films are in the plate-like structure. Also, the SEM photographs in Fig. 2 show that the flexible CuO film surfaces contain shaped grains that aggregate to form plate-like surface morphology. There are similar results of plate-like structure for CuO films produced

**Fig. 1** Schematic illustration of our experimental setup of the SILAR deposition procedure for the deposition of CuO and Ni-doped CuO films. To obtain CuO film, the CA substrates were immersed in the reaction bath for 20 s and then in a cleaning bath (distilled water) for 20 s to remove weakly bound ions. A total of 35 SILAR cycles were performed to synthesize a homogeneous CuO film of the desired thickness

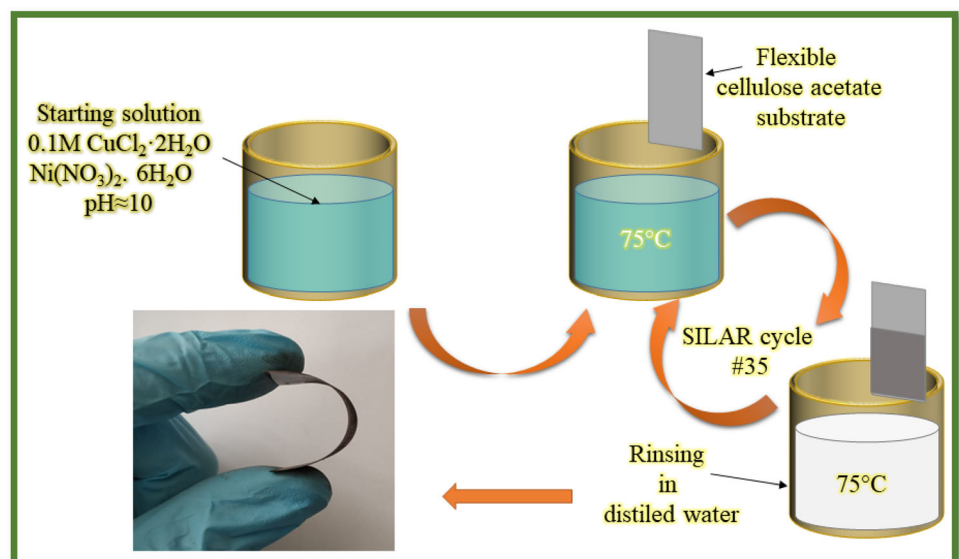
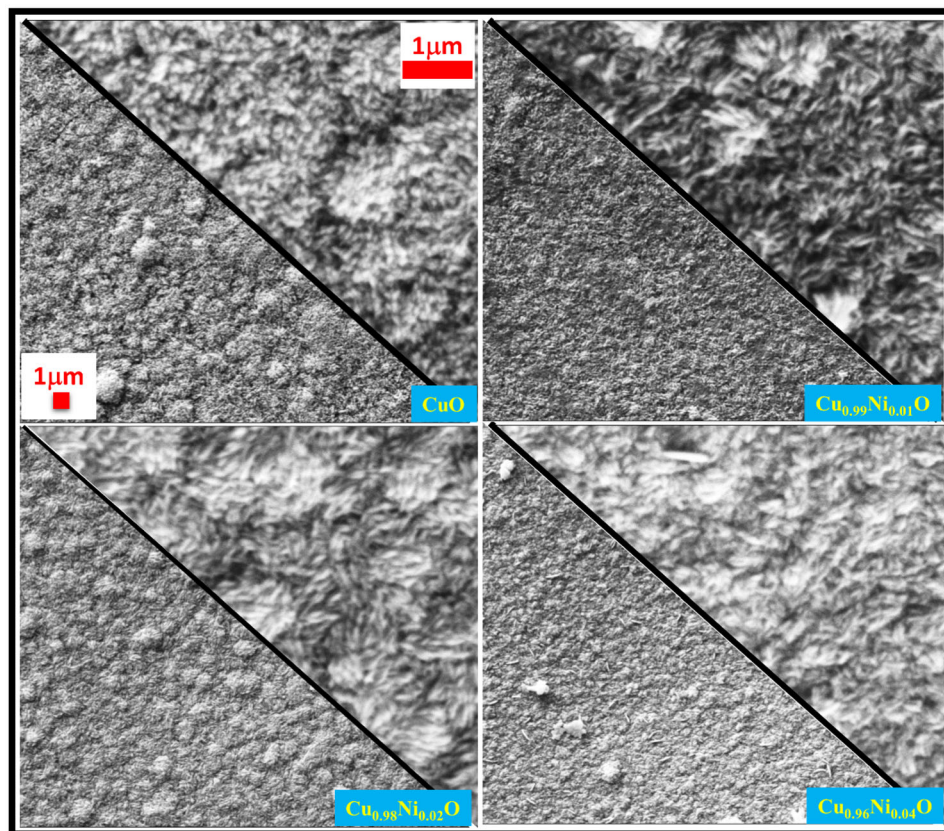


**Fig. 2** SEM images of un-doped and different levels of Ni-doped CuO films on flex substrate. From the SEM photographs, it is seen that the surface morphologies of both un-doped and Ni-doped CuO films are in the plate-like structure



by the SILAR technique [25, 26]. The plate-like structures on the CuO film surfaces vary depending on the Ni doping concentration. These alterations in the surface morphological structure of un-doped and Ni-doped CuO films can be attributed to the relationship between the thermodynamically stable growth, free surface formation nucleation and coalescence process of the films [27–29].

EDX was used to control the content of Ni atoms included, as well as the ratio between Cu and O in the synthesized films. Figure 3 shows the EDX spectrum of elemental analysis of un-doped CuO and  $\text{Cu}_{1-x}\text{Ni}_x\text{O}$  ( $x$ : 0.01, 0.02 and 0.04) films. The substitution of the expected elements to the thin-film structure such as Cu, O, and Ni was observed from the EDX spectrum, which affirms Ni doping on the CuO lattice. Additionally, since the film surfaces are coated with Gold (Au) to increase the conductivity of the films, Au peaks appear in the region between 2 and 3 keV in the EDX spectrum. However, these peaks are not indicated in Fig. 3. Atomic percentage ratios of all CuO films are given in Table 1. The ratio of each element listed in Table 1 makes it clear that Ni is doped in the CuO matrix. It can be seen from the

table that the atomic percentage of Ni increased from 0.70 to 1.40% as the Ni concentration in the solution increased from 1.0 to 4.0%. Diverse electronegativity and ionic radius of precursor salts also influence the growth dynamics in the bath solution, therefore the variation in elemental composition for Cu, Ni, and O for each doping conditions [30, 31].

Elemental mapping was also performed to show the distribution of Cu, O and Ni in the film surface structure. In other words, supplementary confirmation of each element and doping homogeneity in the produced CuO films was performed by EDX mapping as shown in Fig. 4. These mapping images clearly show the homogeneous entity of all possible elements in the films. From the mapping pictures in Fig. 4, the presence of not only Cu (red) and O (green) elements in the  $\text{Cu}_{0.98}\text{Ni}_{0.02}\text{O}$  film, but also Ni (orange) element means that Ni doping is successful.

It is critical to control the film thickness as it has a great influence on the electrical, optical and structural properties of the grown film. As given in Table 2, the thickness values of the CuO films varied between 1.70 and 1.14  $\mu\text{m}$  depending on the increasing Ni concentration. SEM and AFM images also support

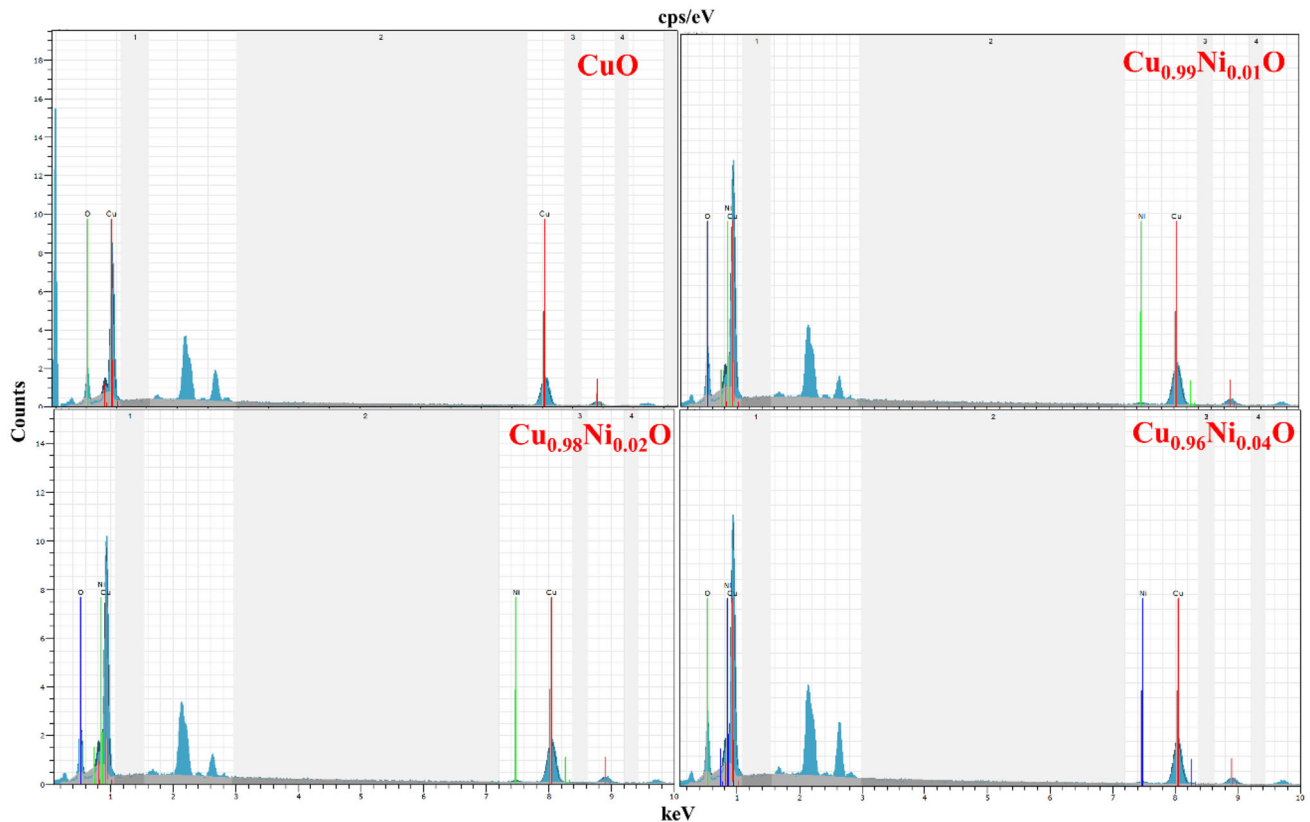


**Fig. 3** Elemental analyses of un-doped CuO and  $\text{Cu}_{1-x}\text{Ni}_x\text{O}$  ( $x$ : 0.01, 0.02 and 0.04) films deposited on CA substrates. The substitution of the expected elements to the thin-film structure such

as Cu, O and Ni was observed from the EDX spectrum, which affirms Ni doping on the CuO lattice

**Table 1** Elemental composition of un-doped CuO and  $\text{Cu}_{1-x}\text{Ni}_x\text{O}$  ( $x$ : 0.01, 0.02 and 0.04) films

Sample name	Cu (at%)	O (at%)	Ni (at%)
CuO	$46.64 \pm 2.33$	$53.36 \pm 2.66$	–
$\text{Cu}_{0.99}\text{Ni}_{0.01}\text{O}$	$37.41 \pm 1.87$	$61.90 \pm 3.09$	$0.70 \pm 0.03$
$\text{Cu}_{0.98}\text{Ni}_{0.02}\text{O}$	$51.13 \pm 2.55$	$47.87 \pm 2.39$	$1.00 \pm 0.05$
$\text{Cu}_{0.96}\text{Ni}_{0.04}\text{O}$	$42.49 \pm 2.12$	$56.12 \pm 2.80$	$1.40 \pm 0.07$

that the surface changes with the film thickness [32, 33]. Surface topologies such as roughness of un-doped CuO and Ni-doped CuO films were investigated with 2D and 3D AFM images, as shown in Fig. 5. It can be seen that the films synthesized from the AFM images are dense, uniform and dispersed on the entire CA substrate with a rough surface. Table 2 shows the mean roughness ( $S_a$ ), root mean square ( $S_q$ ) and entropy values obtained from AFM for the deposited films. As seen in the table,  $S_a$ ,  $S_q$  and entropy values take high values depending on the

doping level of Ni. This change may be due to the accumulation of small grains and the formation of big grains on the film surface as the doping ratio of Ni increases [34, 35]. Additionally, from Table 2, it was observed that the roughness values decreased with the increase in film thickness. This change may be due to the presence of more nucleation sites with increasing film thickness [36, 37].

### 3.2 Microstructural properties

XRD is a significant tool to explore the structural features, crystallite size and can specify the existence of any undesirable impurity phases. Figure 6 denotes the characterization of XRD peaks of CuO and  $\text{Cu}_{1-x}\text{Ni}_x\text{O}$  ( $x$ : 0.01, 0.02 and 0.04) films deposited on flexible CA substrate by using the SILAR technique. The XRD model confirmed that all of the obtained flexible CuO films were polycrystalline in nature. The distinct diffraction lines settled at  $2\theta$  values of  $32.74^\circ$ ,  $35.73^\circ$ ,  $38.71^\circ$ ,  $48.67^\circ$ ,  $52.96^\circ$ ,  $58.13^\circ$ ,  $61.61^\circ$ ,  $65.51^\circ$ , and  $68.31^\circ$ , which correspond to (110),  $(\bar{1}11)$ , (111),  $(\bar{2}02)$ ,

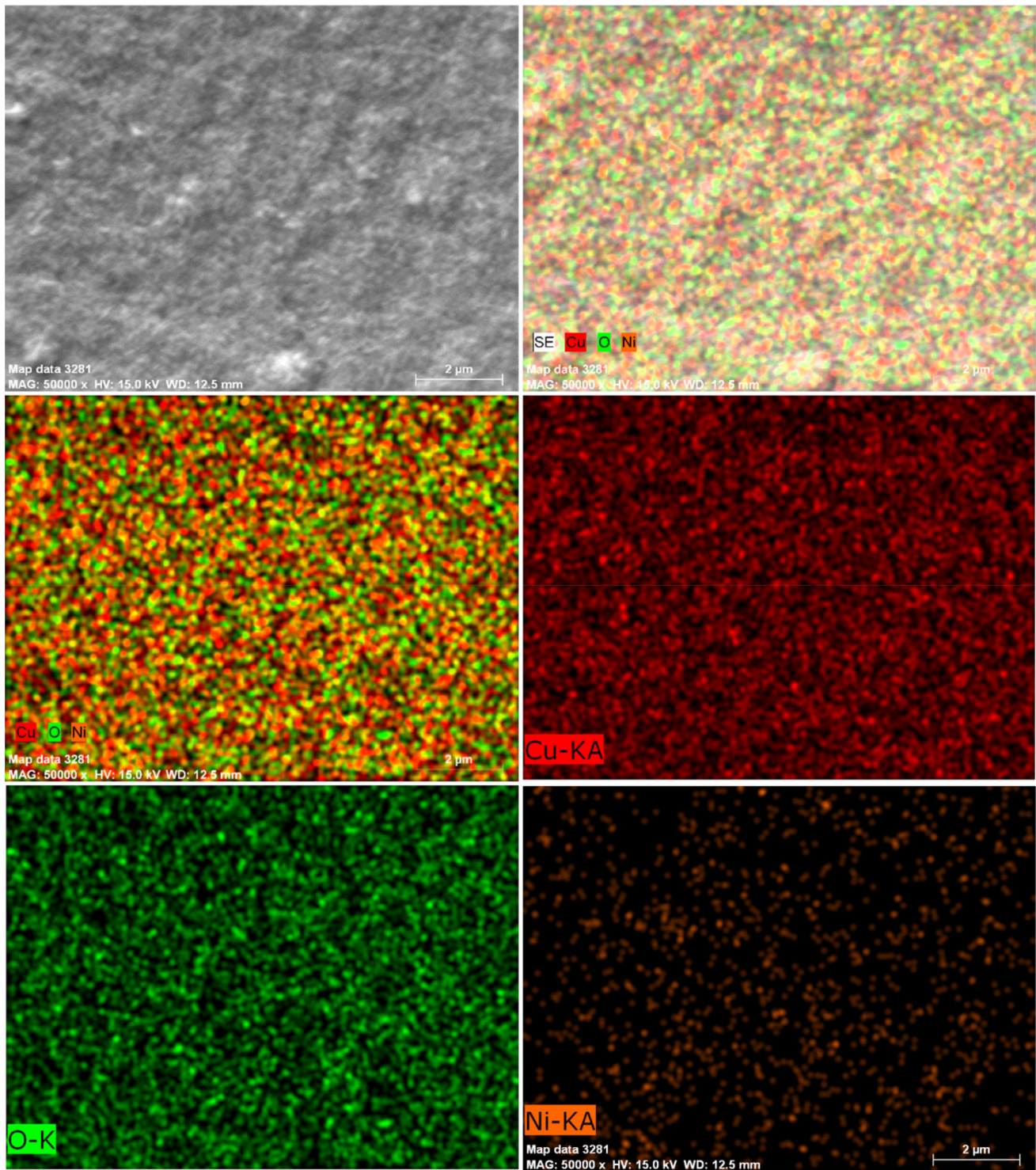


**Fig. 4** EDX mapping analysis images of  $\text{Cu}_{0.98}\text{Ni}_{0.02}\text{O}$  film synthesized on flexible substrate. These mapping images clearly show the homogeneous entity of all possible elements in the films.

(020), (202), ( $\bar{1}13$ ), ( $\bar{3}11$ ) and (220) crystal planes of monoclinic phase the monoclinic structure, respectively (JCPDS card no. 05–0661) [38, 39]. Among these

From the mapping pictures in Fig. 4, the presence of not only Cu (red) and O (green) elements in the  $\text{Cu}_{0.98}\text{Ni}_{0.02}\text{O}$  film, but also Ni (orange) element means that Ni doping is successful (Color figure online)

diffraction peaks, ( $\bar{1}11$ ) and (111) peaks are the most prominent peaks in the XRD model of the synthesized  $\text{CuO}$  films. It obviously presents that the

**Table 2** Average roughness (Sa), root mean square (Sq), entropy and thickness values of CuO and Cu<sub>1-x</sub>Ni<sub>x</sub>O (x: 0.01, 0.02 and 0.04) films

Sample name	Average roughness Sa (nm)	Root mean square Sq (nm)	Entropy	Film thickness (μm)
CuO	34.06	46.01	10.80	1.70
Cu <sub>0.99</sub> Ni <sub>0.01</sub> O	38.96	50.76	10.94	1.64
Cu <sub>0.98</sub> Ni <sub>0.02</sub> O	45.38	59.71	11.16	1.46
Cu <sub>0.96</sub> Ni <sub>0.04</sub> O	94.60	117.77	12.17	1.14

heights of ( $\bar{1}11$ ) and (111) diffraction peaks are much higher than that of other diffraction peaks, which implies a preferential orientation of the constituted crystals along these integrity. The relative intensity values of ( $\bar{1}11$ ) and (111) peaks are listed in Table 3. It is clear from Table 3 that the peak height of CuO films increases with 1.0% Ni concentration and then reduces with increasing Ni concentrations (2.0% and 4.0%) in the solution. The varying peak densities of the CuO films showed that the Ni material significantly affected the film crystallinity [40].

It can be seen from the XRD plot that there are no extra peaks corresponding to Ni or the relevant phase (metallic Ni, NiO) in 1.0% and 2.0% Ni-doped CuO films. This shows that Ni<sup>2+</sup> ions have effectively substituted in Cu<sup>2+</sup> sites without altering the structure of the CuO matrix. This is due to the ionic radius differences between the superseding ion Ni<sup>2+</sup> and the host ion Cu<sup>2+</sup> (Ni<sup>2+</sup>:0.69 Å, Cu<sup>2+</sup>:0.73 Å for coordination number VI) [41, 42]. When the Ni concentration in the solution is 4.0%, it is seen that Ni(OH)<sub>2</sub>-related peaks appear in the Cu<sub>0.96</sub>Ni<sub>0.04</sub>O film. The diffraction peaks at 34.22° and 39.96° were ascribed to the reflections of the planes (100), (101), respectively, of Ni(OH)<sub>2</sub> (JCPDS No: 14-0117) [43, 44].

The average crystallite size (*D*) of the CuO and Cu<sub>1-x</sub>Ni<sub>x</sub>O films was computed using the Scherrer's relationship [45, 46]:

$$D = \frac{0.94\lambda}{\beta \cos\theta} \quad (3)$$

where  $\lambda = 1.5406$  Å is the incident radiation wavelength,  $\beta$  is the full width at half maximum (FWHM) of XRD diffraction peaks and  $\theta$  is the Bragg's diffraction angle, respectively. The obtained values are listed in Table 3. The calculated results show that the crystallite sizes are 12.89, 16.30, 17.13, and 17.88 nm for CuO, Cu<sub>0.99</sub>Ni<sub>0.01</sub>O, Cu<sub>0.98</sub>Ni<sub>0.02</sub>O and Cu<sub>0.96</sub>Ni<sub>0.04</sub>O samples, respectively. In this study, it was found that the *D* raised with increasing Ni

content from 1.0 to 4.0% in aqueous solution. The reason for this change in crystallite size may be that the addition of Ni to the CuO unit cell causes the cell volume to expand, thus causing a strong attractive force between O<sup>2-</sup> ions and Ni<sup>2+</sup> ions and strong repulsive forces with Cu<sup>2+</sup>. Also, the increase with *D* an increase in Ni ratio may be due to conglomeration [47–49].

### 3.3 Molecular properties and FT-IR analysis

Fourier transform infrared (FT-IR) spectroscopy is a useful technique for structural and compositional analysis. FT-IR spectra of un-doped and Ni:CuO on CA flex substrate shown in Fig. 7. Metal-oxide materials generally exhibit unique absorption bands in the fingerprint region resulting from stretching vibrations, but, also in here, strong absorption peaks of CA as well as CuO were observed together in all spectra because of the penetration depth of IR. The FT-IR spectrum of un-doped CuO on the CA substrate presented three typical intense peaks incorporated with the Cu–O vibrations of monoclinic CuO at 420 cm<sup>-1</sup>, 491 cm<sup>-1</sup> and 615 cm<sup>-1</sup> [50–52]. The position of the absorption peak (615 cm<sup>-1</sup>) in the fingerprint region is usually attributed to the presence of Cu<sub>2</sub>O, but traces of Cu<sub>2</sub>O were not seen in the XRD spectra. When these values were compared with those previously reported, it was observed that two absorption peaks at low wavelengths were slightly blue-shifted and the higher one was red-shifted [52, 53]. These shifts are usually attributed to the decrease in the surface area and surface defects and significant changes with doping [51, 54, 55].

CA, among other peaks, has the presence of three important peaks belonging to acetyl group vibrations at 1732 cm<sup>-1</sup> ( $\nu_{C=O}$ ), 1327 cm<sup>-1</sup> ( $\nu_{-CH_3}$ ), and 1248 cm<sup>-1</sup> ( $\nu_{C-O}$ ) [50, 56, 57]. Because of the acetylation process, the peaks of the –OH functional groups

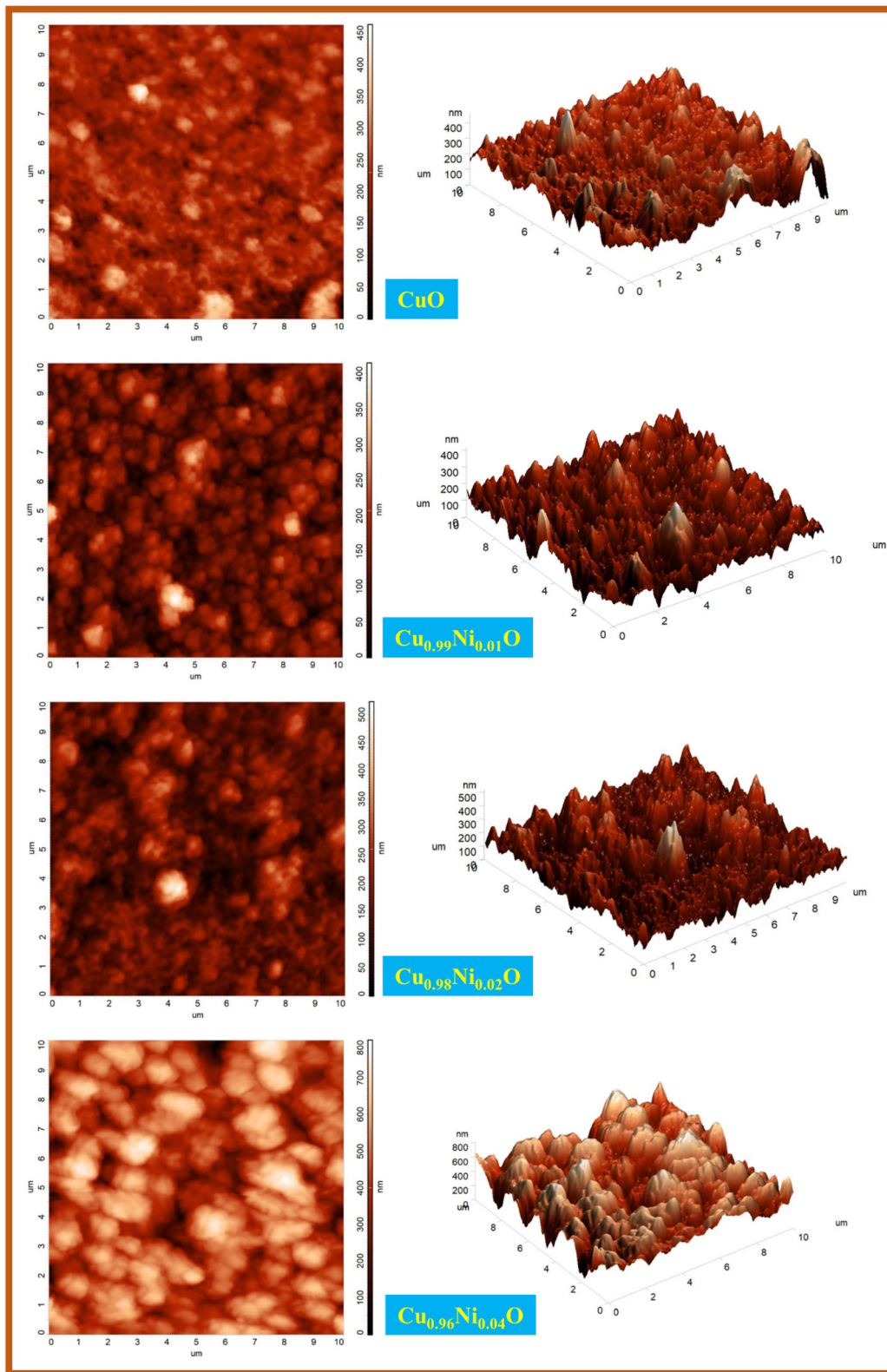


**Fig. 5** 2D and 3D AFM images of un-doped and Ni-doped CuO films on flex substrate over a scan area of  $10\ \mu\text{m} \times 10\ \mu\text{m}$ . It can be seen that the films synthesized from the AFM images are dense, uniform and dispersed on the entire CA substrate with a rough surface



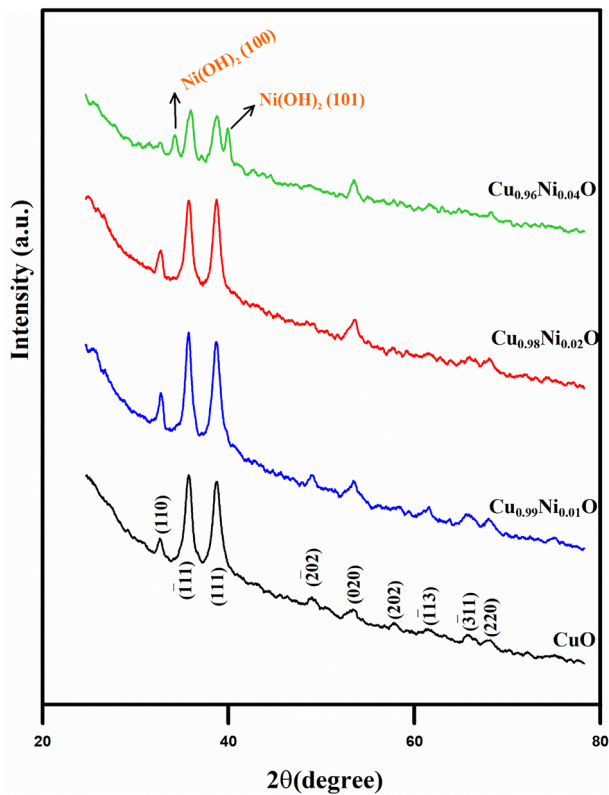


**Fig. 6** X-ray diffraction patterns of un-doped and Ni-doped CuO films on flex substrate. The XRD model confirmed that all of the obtained flexible CuO films were polycrystalline in nature. The varying peak densities of the CuO films showed that the Ni material significantly affected the film crystallinity

were reduced and were not observed in the spectrum [56]. No shift was observed in the main peaks of CA, indicating that the CuO and Ni-doped CuO films did not react with the substrate. Also, FT-IR spectrum of Ni-doped CuO on CA has an absorption band at  $2357\text{ cm}^{-1}$  due to the antisymmetric stretching mode of vibrations of  $\text{CO}_2$  molecules adsorbed from air [45, 58]. This situation can be explained as a because of growing clusters with the doping of Ni ions causes form a structure with larger spaces between clusters. This is confirmed by the RMS values obtained via AFM and the increasing thickness values (Table 2).

**Table 3** Relative peak intensity, crystallite size and bandgap values of CuO and  $\text{Cu}_{1-x}\text{Ni}_x\text{O}$  ( $x$ : 0.01, 0.02 and 0.04) films

Sample name	Relative peak intensity (cps)		Crystallite size (nm)	Bandgap (eV)
	( $\bar{1}11$ )	(111)		
CuO	220	265	$12.89 \pm 0.11$	1.48
$\text{Cu}_{0.99}\text{Ni}_{0.01}\text{O}$	323	272	$16.30 \pm 0.31$	1.56
$\text{Cu}_{0.98}\text{Ni}_{0.02}\text{O}$	279	227	$17.13 \pm 0.13$	1.63
$\text{Cu}_{0.96}\text{Ni}_{0.04}\text{O}$	145	123	$17.88 \pm 0.12$	1.69

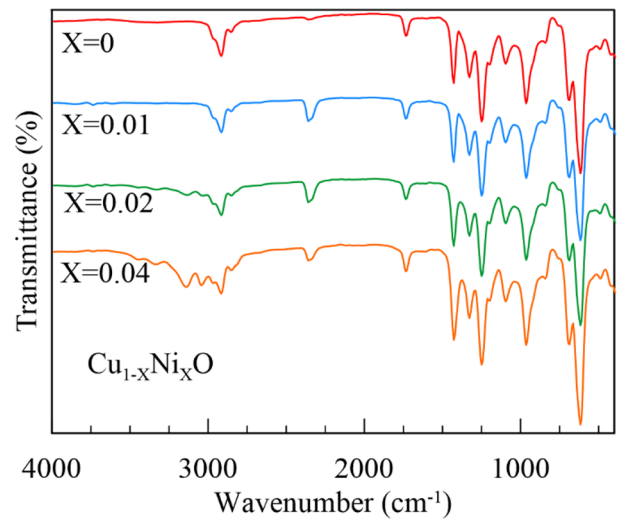


**Fig. 7** FT-IR spectrum of un-doped CuO and  $\text{Cu}_{1-x}\text{Ni}_x\text{O}$  ( $x = 0.01, 0.02$  and  $0.04$ )-doped CuO thin films on flexible CA substrate. Metal-oxide materials generally exhibit unique absorption bands in the fingerprint region resulting from stretching vibrations, but, also in here, strong absorption peaks of CA as well as CuO were observed together in all spectra because of the penetration depth of IR

### 3.4 Optical properties

The optical bandgap energy for all pure and Ni-doped CuO films was determined according to the Tauc expression [59, 60].

$$\alpha h\nu = C(h\nu - E_g)^n \quad (4)$$

In this Tauc equation,  $\alpha$ ,  $h\nu$ ,  $C$  and  $E_g$  are the absorption coefficient, the photon energy, a constant, and the optical bandgap. Also,  $n$  is  $\frac{1}{2}$  for direct allowed transitions [61, 62]. A graph is drawn between  $(\alpha h\nu)^2$  and  $h\nu$  the points where the drawn tangents intersect the horizontal axis ( $h\nu$  axis,  $y = 0$ ) to give the bandgap energy value as shown in Fig. 8. The optical bandgap was found to be 1.48 eV for the un-doped CuO film and this value is in good accordance with other studies [63, 64]. Figure 8 shows that the  $E_g$  of Ni-incorporated samples improves with

increasing Ni ratio. The  $E_g$  results are tabulated in Table 3 and were estimated to be 1.48, 1.56, 1.63, and 1.69 eV, respectively, for CuO, Cu<sub>0.99</sub>Ni<sub>0.01</sub>O, Cu<sub>0.98</sub>Ni<sub>0.02</sub>O, and Cu<sub>0.96</sub>Ni<sub>0.04</sub>O films. Due to the wide bandgap (3.6–4.0 eV) of NiO films [65], the doping of Ni on CuO will increase the bandgap of Cu<sub>1-x</sub>Ni<sub>x</sub>O ( $x$ : 0.01, 0.02 and 0.04) films. This increment in bandgap after Ni doping to CuO may be due to Ni replacement at the Cu sites in the CuO matrix. Moreover, this augmentation may be ascribed to different agents, mainly oxygen stoichiometry, quantum confinement, and quantum size effect [66–68].

Figure 9 demonstrates the optical transmittance plot against the wavelength of the deposited un-doped and Ni-doped CuO films. All the films obtained show good transmittance and are recorded in the wavelength range of 300–1100 nm. The transmittance values alter between 11 and 37%, depending on the Ni dopant concentration. From the graph, it was found that the transmission for the un-doped CuO film was about 11% and increased with rising Ni level. This alteration in the transmittance of samples

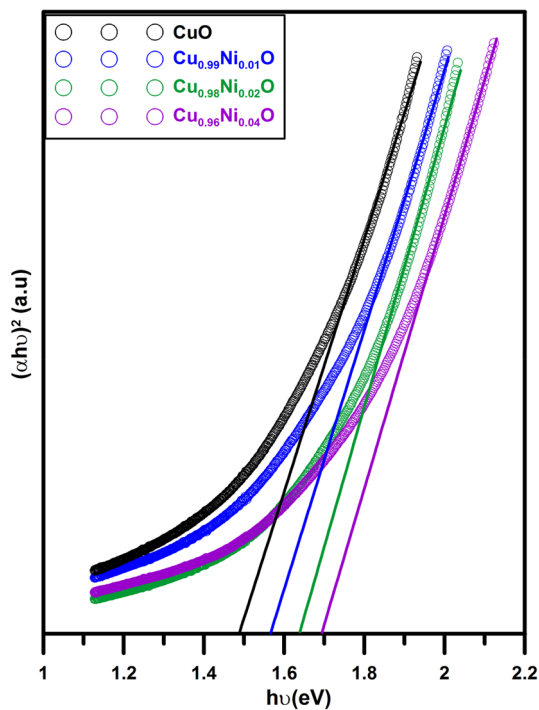


**Fig. 8** Comparison of  $(\alpha hv)^2$  versus  $h\nu$  plots of un-doped CuO and Ni-doped CuO thin films on flexible substrate. The optical bandgap was found to be 1.48 eV for the un-doped CuO film and the  $E_g$  of Ni-incorporated samples improves with increasing Ni ratio

is due to the difference in the thickness of the samples. Generally, the transmittance of these films shows a significant increase with a decrease in film thickness. This variation is due to the thickness effect (Beer–Lambert’s law), where light is increasingly adsorbed in a material originating from longer optical paths. Also, the reason for the change in the transmittance of the films may be related to the crystal defects and the changing size (crystal size) [69–71].

### 3.5 DC-electrical properties

The electrical properties of un-doped CuO and Ni-doped CuO films on a flexible substrate were characterized using sheet resistivity measurements. This is because the resistivity of a thin film depends strongly on the nature of its not to bulk properties. Two-probe technique was used to measure the dc-electrical resistivity of un-doped and Ni-doped films. Silver paste was used to make Ohmic contacts with CuO thin films and the applied bias between two conductive electrodes was 10 V. DC resistivity values were calculated using Ohm’s law,  $R = V/I$ , where  $R$  is the resistance,  $V$  is the applied bias and  $I$  is the measured current. Sheet resistance  $R_{sh}$  was calculated using the following equation [72];

$$R_{sh} = \frac{wd}{l} R \tag{5}$$

where  $w$  is the gap between the electrodes,  $d$  is the film thickness and  $l$  is the length of the electrodes.

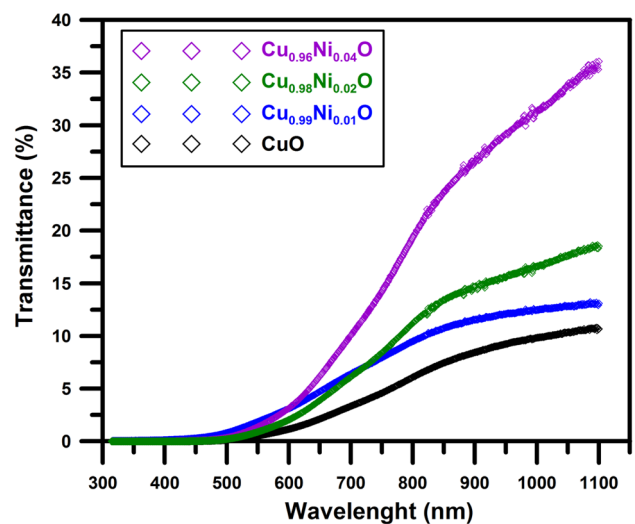


**Fig. 9** Optical transmittance spectra un-doped CuO and Ni-doped CuO thin films on flexible substrate. The transmittance values alter between 11 and 37%, depending on the Ni dopant concentration

Table 4. shows that the sheet resistance increases with the doping ratio and decreases with increasing film thickness. The effect of thickness on sheet resistance cannot be explained because of the decrease in grain boundaries causing lower resistance. This increment could be explained by the increase in impurity scattering at the grain boundaries due to Ni-incorporation and latter change of optical energy gap [73–75]. Also, CuO is a low-mobility p-type semiconductor and the incorporation of Ni results in an increase the native defects. Therefore, a higher hole concentration and scattering of holes at the native defects correspond to lower mobility and higher resistivity [76].

We have studied on resistivity values at bending conditions to examine the flexibility of CuO and Ni:CuO thin films built on flex substrate. To for this, films were folded onto a 4 cm diameter cylinder and the sheet resistances of the films were calculated under the new conditions (insets in Fig. 10). The sheet resistance values of thin films slightly increased (Fig. 10). This phenomenon can be interconnected with the variation in mobility stimulated by the lattice decoration due to the piezoresistive effect in the thin film [77–79]. Conventionally, the conductivity of p-type semiconductors decreases linearly (as in here) because of the strain owing to the increase in the hole population with decreased mobility by the deformation. Also, such thin films built on flexible substrates tend to become brittle and form fractures during bending.

The changes in the dc resistivity can be characterized using the ratio of the resistance to ( $R_{sh}$ ) and after bending ( $R_{sh}^*$ ) (i.e.  $S = R_{sh}/R_{sh}^*$ ) [21]. The convergence of this ratio to unity simplifies device fabrication, while moving away from this value will have undesirable effects on sensor properties. In here, this ratio changes between the 1.14 and 1.17 for CuO and  $Cu_{0.96}Ni_{0.04}O$ , respectively. Although this value is slightly high, it is lower than the sensing response parameter compared to similar studies [2, 80, 81].

**Table 4** Sheet resistance and resistivity values of CuO and  $Cu_{1-x}Ni_xO$  ( $x$ : 0.01, 0.02 and 0.04) films

Sample name	Normal		Bending	
	Resistivity $\times 10^4 \Omega \text{ cm}$	Sheet resistance $R_{sh} (\times 10^8 \Omega/\text{sq.})$	Resistivity $\times 10^4 \Omega \text{ cm}$	Sheet resistance $R_{sh} (\times 10^8 \Omega/\text{sq.})$
CuO	4.66	2.7	5.47	3.1
$Cu_{0.99}Ni_{0.01}O$	32.22	19.6	37.61	22.9
$Cu_{0.98}Ni_{0.02}O$	31.40	21.5	36.41	24.9
$Cu_{0.96}Ni_{0.04}O$	27.87	24.4	31.84	27.9

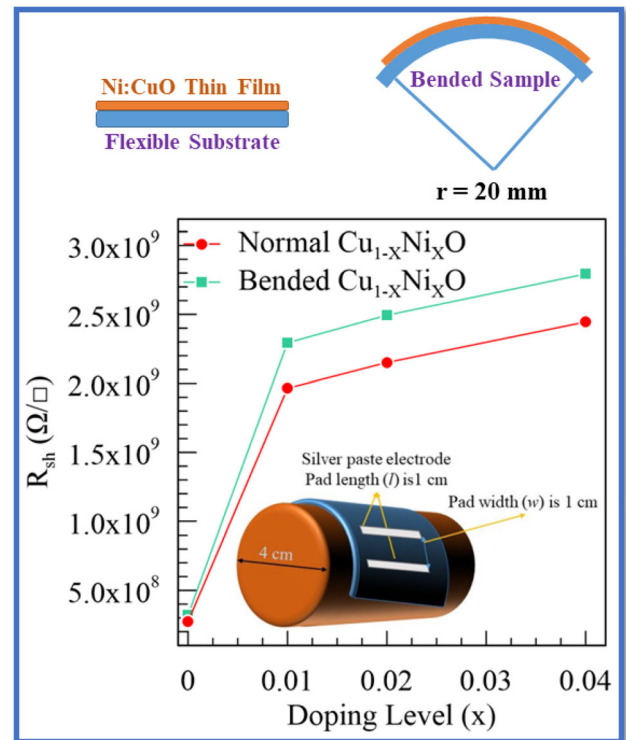


**Fig. 10** Sheet resistance versus doping level graphs of  $Cu_{1-x}Ni_xO$  films. Inset shows the bending conditions and contact properties. The sheet resistance values of thin films slightly increased with bending condition. This phenomenon can be interconnected with the variation in mobility stimulated by the lattice decoration due to the piezoresistive effect in the thin film

## 4 Conclusions

Nanostructured flexible CuO films with varied ratios of transition metal Ni were synthesized by the SILAR technique on cellulose acetate substrates. From the SEM images, it is seen that the surface morphologies of both un-doped and Ni-doped CuO films are in the nanorod structure. The substitution of the expected elements to the thin-film structure such as Cu, O, and Ni was observed from the EDX spectrum, which affirms Ni doping on the CuO lattice. The XRD model

confirmed that all of the obtained flexible CuO films were polycrystalline in nature. The FT-IR spectrum of samples on the CA substrate showed three characteristic strong peaks associated with the Cu–O vibrations of monoclinic CuO. The optical energy gaps of different flexible CuO films prepared from different Ni concentrations 1.0%, 2.0%, and 4.0%, were calculated as 1.56 eV, 1.63 eV, and 1.69 eV, respectively. This increment in bandgap after Ni doping to CuO may be due to Ni replacement at the Cu sites in the CuO matrix. Two-probe technique was used to measure the dc-electrical resistivity of undoped and Ni-doped films. Obtained results show that the sheet resistance increases with the Ni doping ratio and decreases with increasing film thickness. This is because the resistivity of a thin film depends strongly on the nature of its not to bulk properties. Additionally, we have examined the resistivity values at bending conditions to examine the flexibility of CuO thin films for bending radius  $\sim 20$  mm. The sheet resistance values of thin films slightly increased because of bending. This phenomenon can be related to the change in mobility induced by the lattice deformation due to the piezoresistive effect in the thin film. These obtained results for light-weight and flexible CuO thin-film materials make them ideal for a wide variety of applications unsuitable for heavy thin films.

### Author contributions

All authors contributed to the study conception and design. Material preparation, data collection and analysis were performed by RA, AA and BŞ. The first draft of the manuscript was written by BŞ and all authors commented on previous versions of the manuscript. All authors read and approved the final manuscript.

### Funding

The authors declare that no funds, grants or other support were received during the preparation of this manuscript.

### Data availability

The data that support the findings of this study are available on request from the corresponding author.

### Declarations

**Competing interests** The authors have no relevant financial or non-financial interests to disclose.

### References

1. S. Khan, S. Ali, A. Bermak, Recent developments in printing flexible and wearable sensing electronics for healthcare applications. *Sensors-Basel* **19**(5), 1230 (2019)
2. B. Şahin, Flexible nanostructured CuO thin film: a promising candidate for wearable real-time sweat rate monitoring devices. *Sens. Actuators A* **341**, 113604 (2022)
3. W. Maziarz, TiO<sub>2</sub>/SnO<sub>2</sub> and TiO<sub>2</sub>/CuO thin film nano-heterostructures as gas sensors. *Appl. Surf. Sci.* **480**, 361–370 (2019)
4. R. Rai, Study of structural and electrical properties of pure and Zn-Cu doped SnO<sub>2</sub>. *Adv. Mater. Lett.* **1**(1), 55–58 (2010)
5. S.R. Gawali, V.L. Patil, V.G. Deonikar, S.S. Patil, D.R. Patil, P.S. Patil, J. Pant, Ce doped NiO nanoparticles as selective NO<sub>2</sub> gas sensor. *J. Phys. Chem. Solids* **114**, 28–35 (2018)
6. S. Baturay, I. Candan, C. Ozaydin, Structural, optical, and electrical characterizations of Cr-doped CuO thin films. *J. Mater. Sci.: Mater. Electron.* **33**(9), 7275–7287 (2022)
7. R. Bekkari, B. Jaber, L. Laâ nab, Effect of monovalent dopant ionic radius and concentration on the growth orientation and optical properties of the sol–gel-derived ZnO thin films. *J. Mater. Sci.: Mater. Electron.* **33**(15), 12126–12136 (2022)
8. B. Sakthivel, L. Manjakkal, G. Nammalvar, High performance CuO nanorectangles-based room temperature flexible NH<sub>3</sub> sensor. *IEEE Sens. J.* **17**(20), 6529–6536 (2017)
9. A.S.A. Raj, V. Biju, Nanostructured CuO: facile synthesis, optical absorption and defect dependent electrical conductivity. *Mater. Sci. Semicond. Process.* **68**, 38–47 (2017)
10. H. Khmissi, A.M. El Sayed, M. Shaban, Structural, morphological, optical properties and wettability of spin-coated copper oxide; influences of film thickness, Ni, and (La, Ni) co-doping. *J. Mater. Sci.* **51**(12), 5924–5938 (2016)
11. H. Safdar, R. Aydın, B. Şahin, Syntheses, structural evolution, electrical and optoelectronic characterization of ZnO/CuO composite films doped with transition metal Mn<sup>2+</sup> ions. *Ceram. Int.* **48**(18), 26678–26688 (2022)
12. S. Dolai, R. Dey, S. Das, S. Hussain, R. Bhar, A.K. Pal, Cupric oxide (CuO) thin films prepared by reactive d.c.

- magnetron sputtering technique for photovoltaic application. *J. Alloy. Compd.* **724**, 456–464 (2017)
13. V. Dhanasekaran, T. Mahalingam, R. Chandramohan, J.-K. Rhee, J.P. Chu, Electrochemical deposition and characterization of cupric oxide thin films. *Thin Solid Films* **520**(21), 6608–6613 (2012)
  14. J. Morales, L. Sánchez, F. Martín, J.R. Ramos-Barrado, M. Sánchez, Use of low-temperature nanostructured CuO thin films deposited by spray-pyrolysis in lithium cells. *Thin Solid Films* **474**(1), 133–140 (2005)
  15. A. Moumen, B. Hartiti, E. Comini, Z. El Khalidi, H.M.M.M. Arachchige, S. Fadili, P. Thevenin, Preparation and characterization of nanostructured CuO thin films using spray pyrolysis technique. *Superlattice Microstruct.* **127**, 2–10 (2019)
  16. S.K. Shinde, S.M. Mohite, A.A. Kadam, H.M. Yadav, G.S. Ghodake, K.Y. Rajpure, D.S. Lee, D.Y. Kim, Effect of deposition parameters on spray pyrolysis synthesized CuO nanoparticle thin films for higher supercapacitor performance. *J. Electroanal. Chem.* **850**, 113433 (2019)
  17. M.R. Das, A. Mukherjee, P. Maiti, S. Das, P. Mitra, Studies on multifunctional properties of SILAR synthesized CuO thin films for enhanced supercapacitor, photocatalytic and ethanol sensing applications. *J. Electron. Mater.* **48**(5), 2718–2730 (2019)
  18. A. Akkaya, O. Kahveci, R. Aydın, B. Şahin, Amplifying main physical characteristics of CuO films using ascorbic acid as the reducer and stabilizer agent. *Appl. Phys. A* **127**(12), 911 (2021)
  19. D. Baran, D. Corzo, G. Blazquez, Flexible electronics: status, challenges and opportunities. *Front. Electron.* (2020). <http://doi.org/10.3389/felec.2020.594003>
  20. M.J. Cordill, P. Kreiml, C. Mitterer, Materials engineering for flexible metallic thin film applications. *Materials* **15**(3), 926 (2022)
  21. H. Kim, S. Park, Y. Park, D. Choi, B. Yoo, C.S. Lee, Fabrication of a semi-transparent flexible humidity sensor using kinetically sprayed cupric oxide film. *Sens. Actuators B* **274**, 331–337 (2018)
  22. Y. Khan, A. Thielens, S. Muin, J. Ting, C. Baumbauer, A.C. Arias, A new frontier of printed electronics: flexible hybrid electronics. *Adv. Mater.* **32**(15), 1905279 (2020)
  23. N. Luo, W. Dai, C. Li, Z. Zhou, L. Lu, C.C.Y. Poon, S.-C. Chen, Y. Zhang, N. Zhao, Flexible piezoresistive sensor patch enabling ultralow power cuffless blood pressure measurement. *Adv. Funct. Mater.* **26**(8), 1178–1187 (2016)
  24. C.M. Muiva, A.O. Juma, L.M. Lepodise, K. Maabong, D. Letsholathebe, Surfactant assisted chemical bath deposition based synthesis of 1-D nanostructured CuO thin films from alkaline baths. *Mater. Sci. Semicond. Process.* **67**, 69–74 (2017)
  25. G. Yıldırım, E. Yücel, Variation of the key structural, morphological, and optical properties of nanostructured copper(II) oxide (CuO) thin films using surfactant CAPB as a capping agent. *J. Mater. Sci.: Mater. Electron.* **33**(24), 19057–19070 (2022)
  26. B. Şahin, T. Kaya, Enhanced hydration detection properties of nanostructured CuO films by annealing. *Microelectron. Eng.* **164**, 88–92 (2016)
  27. J.-W. Ha, J. Oh, H. Choi, H. Ryu, W.-J. Lee, J.-S. Bae, Photoelectrochemical properties of Ni-doped CuO nanorods grown using the modified chemical bath deposition method. *J. Ind. Eng. Chem.* **58**, 38–44 (2018)
  28. J. Oh, H. Ryu, W.-J. Lee, J.-S. Bae, Improved photostability of a CuO photoelectrode with Ni-doped seed layer. *Ceram. Int.* **44**(1), 89–95 (2018)
  29. J. Uddin, M. Sharmin, M.N. Hasan, J. Podder, Influence of Ni doping on the morphological, structural, optical and electrical properties of CuO thin films deposited via a spray pyrolysis. *Opt. Mater.* **119**, 111388 (2021)
  30. D. Son, S. Cho, J. Nam, H. Lee, M. Kim, X-ray-based spectroscopic techniques for characterization of polymer nanocomposite materials at a molecular level. *Polymers* **12**(5), 1053 (2020)
  31. X. Ji, Relative effect of electronegativity on formation of high entropy alloys. *Int. J. Cast Met. Res.* **28**(4), 229–233 (2015)
  32. V. Dhanasekaran, T. Mahalingam, Surface modifications and optical variations of (–111) lattice oriented CuO nanofilms for solar energy applications. *Mater. Res. Bull.* **48**(9), 3585–3593 (2013)
  33. S. Visalakshi, R. Kannan, S. Valanarasu, A. Kathalingam, S. Rajashabala, Studies on optical and electrical properties of SILAR-deposited CuO thin films. *Mater. Res. Innov.* **21**(3), 146–151 (2017)
  34. M. Ayachi, F. Ayad, A. Djelloul, L. Benharrat, S. Anas, Synthesis and characterization of Ni-doped ZnO thin films prepared by sol-gel spin-coating method. *Semiconductors* **55**(5), 482–490 (2021)
  35. A. Abdel-Galil, N.L. Moussa, I.S. Yahia, Study on spray deposited Ni-doped CuO nanostructured thin films: microstructural and optical behavior. *J. Mater. Sci.: Mater. Electron.* **33**(8), 4984–4999 (2022)
  36. R.K. Pandey, K. Ghosh, S. Mishra, J.P. Bange, P.K. Bajpai, D.K. Gautam, Effect of film thickness on structural and optical properties of sol-gel spin coated aluminum doped zinc oxide (Al:ZnO) thin films. *Mater. Res. Express* **5**(8), 086408 (2018)

37. D. Raoufi, F. Hosseinpanahi, The effect of film thickness on surface morphology of ITO thin films. *J. Theor. Appl. Phys.* **7**(1), 21 (2013)
38. B. Karthikeyan, Raman spectral probed electron–phonon coupling and phonon lifetime properties of Ni-doped CuO nanoparticles. *Appl. Phys. A* **127**(3), 205 (2021)
39. N.M. Basith, J.J. Vijaya, L.J. Kennedy, M. Bououdina, Structural, morphological, optical, and magnetic properties of Ni-doped CuO nanostructures prepared by a rapid microwave combustion method. *Mater. Sci. Semicond. Process.* **17**, 110–118 (2014)
40. M.A. Asghar, A. Ali, A. Haider, M. Zaheer, T. Nisar, V. Wagner, Z. Akhter, Electrochemically deposited amorphous cobalt–nickel-doped copper oxide as an efficient electrocatalyst toward water oxidation reaction. *ACS Omega* **6**(30), 19419–19426 (2021)
41. S.P. Kamble, V.D. Mote, Optical and room-temperature ferromagnetic properties of Ni-doped CuO nanocrystals prepared via auto-combustion method. *J. Mater. Sci.: Mater. Electron.* **32**(5), 5309–5315 (2021)
42. P. Arunachalam, S. Nagarani, S. Prasad, M.S. AlSalhi, A.M. Al-Mayouf, A.M. Moydeen, S. Ganapathy, Facile coprecipitation synthesis of nickel doped copper oxide nanocomposite as electrocatalyst for methanol electrooxidation in alkaline solution. *Mater. Res. Express* **5**(1), 015512 (2018)
43. D. Wang, R. Xu, X. Wang, Y. Li, NiO nanorings and their unexpected catalytic property for CO oxidation. *Nanotechnology* **17**(4), 979–983 (2006)
44. A. Sreenavya, T. Baskaran, V. Ganesh, D. Sharma, N. Kulal, A. Sakthivel, Framework of ruthenium-containing nickel hydroxalcalite-type material: preparation, characterisation, and its catalytic application. *RSC Adv.* **8**(44), 25248–25257 (2018)
45. A. Taşdemir, R. Aydin, A. Akkaya, N. Akman, Y. Altınay, H. Çetin, B. Şahin, A. Uzun, E. Ayyıldız, A green approach for the preparation of nanostructured zinc oxide: characterization and promising antibacterial behaviour. *Ceram. Int.* **47**(14), 19362–19373 (2021)
46. P. Scherrer, Bestimmung der Größe und der inneren Struktur von Kolloidteilchen mittels Röntgenstrahlen. *Nachr. Ges. Wiss. Göttingen*, 98–100 (1918)
47. M. Chandrasekar, M. Subash, S. Logambal, G. Udhayakumar, R. Uthrakumar, C. Inmozhi, W.A. Al-Onazi, A.M. Al-Mohaimed, T.-W. Chen, K. Kanimozhi, Synthesis and characterization studies of pure and Ni doped CuO nanoparticles by hydrothermal method. *J. King Saud Univ. Sci.* **34**(3), 101831 (2022)
48. A.M. Alsaad, A.A. Ahmad, Q.M. Al-Bataineh, A.A. Bani-Salameh, H.S. Abdullah, I.A. Qattan, Z.M. Al-Bataineh, A.D. Telfah, Optical, structural, and crystal defects characterizations of dip synthesized (Fe-Ni) co-doped ZnO thin films. *Materials* **13**(7), 1737 (2020)
49. I. Muniyandi, G.K. Mani, P. Shankar, J.B.B. Rayappan, Effect of nickel doping on structural, optical, electrical and ethanol sensing properties of spray deposited nanostructured ZnO thin films. *Ceram Int* **40**(6), 7993–8001 (2014)
50. L.M. Dwivedi, N. Shukla, K. Baranwal, S. Gupta, S. Siddique, V. Singh, Gum acacia modified Ni doped CuO nanoparticles: an excellent antibacterial material. *J. Clust. Sci.* **32**(1), 209–219 (2021)
51. R.N. Mariammal, K. Ramachandran, G. Kalaiselvan, S. Arumugam, B. Renganathan, D. Sastikumar, Effect of magnetism on the ethanol sensitivity of undoped and Mn-doped CuO nanoflakes. *Appl. Surf. Sci.* **270**, 545–552 (2013)
52. K. Borgohain, J.B. Singh, M.V. Rama Rao, T. Shripathi, S. Mahamuni, Quantum size effects in CuO nanoparticles. *Phys. Rev. B* **61**(16), 11093–11096 (2000)
53. G. Kliche, Z.V. Popovic, Far-infrared spectroscopic investigations on CuO. *Phys. Rev. B* **42**(16), 10060–10066 (1990)
54. L.-J. Chen, G.-S. Li, L.-P. Li, CuO nanocrystals in thermal decomposition of ammonium perchlorate: stabilization, structural characterization and catalytic activities. *J. Therm. Anal. Calorim.* **91**(2), 581–587 (2008)
55. A. Kumar, M. Kumar, P. Chandra Sati, M.K. Srivastava, S. Ghosh, S. Kumar, Structural, magnetic and optical properties of diluted magnetic semiconductor (DMS) phase of Ni modified CuO nanoparticles. *Curr. Appl. Phys.* **32**, 24–35 (2021)
56. P. Fei, L. Liao, B. Cheng, J. Song, Quantitative analysis of cellulose acetate with a high degree of substitution by FTIR and its application. *Anal. Methods-UK* **9**(43), 6194–6201 (2017)
57. D. Tristantini, A. Yunan, Advanced characterization of microbeads replacement from cellulose acetate based on empty fruit bunches and dried jackfruit leaves. *E3S Web Conf.* **67**, 04045 (2018)
58. G. Richner, G. Puxty, Assessing the chemical speciation during CO<sub>2</sub> absorption by aqueous amines using in situ FTIR. *Ind. Eng. Chem. Res.* **51**(44), 14317–14324 (2012)
59. B. Şahin, R. Aydin, H. Cetin, Tuning the morphological, structural, optical and dielectric properties of hausmannite (Mn<sub>3</sub>O<sub>4</sub>) films by doping heavy metal lead. *Superlattice Microstruct.* **143**, 106546 (2020)
60. J.I. Pankove, *Optical Processes in Semiconductors* (Dover Publications, Mineola, 2012)
61. M.H. Babu, J. Podder, B.C. Dev, M. Sharmin, p to n-type transition with wide blue shift optical band gap of spray synthesized Cd doped CuO thin films for optoelectronic device applications. *Surf. Interfaces* **19**, 100459 (2020)

62. N. Thakur, Anu, K. Kumar, Effect of (Ag, Co) co-doping on the structural and antibacterial efficiency of CuO nanoparticles: a rapid microwave assisted method. *J. Environ. Chem. Eng.* **8**(4), 104011 (2020)
63. O. Daoudi, Y. Qachaou, A. Raidou, K. Nouneh, M. Lharch, M. Fahoume, Study of the physical properties of CuO thin films grown by modified SILAR method for solar cells applications. *Superlattice Microstruct.* **127**, 93–99 (2019)
64. H. Siddiqui, M.R. Parra, M.S. Qureshi, M.M. Malik, F.Z. Haque, Studies of structural, optical, and electrical properties associated with defects in sodium-doped copper oxide (CuO/Na) nanostructures. *J. Mater. Sci.* **53**(12), 8826–8843 (2018)
65. K. Varunkumar, R. Hussain, G. Hegde, A.S. Ethiraj, Effect of calcination temperature on Cu doped NiO nanoparticles prepared via wet-chemical method: structural, optical and morphological studies. *Mater. Sci. Semicond. Process.* **66**, 149–156 (2017)
66. S. Al-Amri, M. Shah Nawaze Ansari, S. Rafique, M. Aldhahri, S. Rahimuddin, A. Azam, A. Memic, Ni doped CuO nanoparticles: structural and optical characterizations. *Curr. Nanosci.* **11**(2), 191–197 (2015)
67. W. Yin, J. Yang, K. Zhao, A. Cui, J. Zhou, W. Tian, W. Li, Z. Hu, J. Chu, High responsivity and external quantum efficiency photodetectors based on solution-processed Ni-doped CuO films. *ACS Appl. Mater. Interfaces* **12**(10), 11797–11805 (2020)
68. H. El Aakib, J.F. Pierson, M. Chaik, H. Ait Dads, C. Samba Vall, A. Narjis, A. Outzourhit, Nickel doped copper oxide thin films prepared by radiofrequency reactive sputtering: study of the impact of nickel content on the structural, optical and electrical properties. *Spectrosc. Lett.* **54**(7), 487–494 (2021)
69. F. Mukhtar, T. Munawar, M.S. Nadeem, M. Hasan, F. Husain, M.A. Nawaz, F. Iqbal, Multi metal oxide NiO-Fe<sub>2</sub>O<sub>3</sub>-CdO nanocomposite-synthesis, photocatalytic and antibacterial properties. *Appl. Phys. A* **126**(8), 588 (2020)
70. D.-C. Tsai, Z.-C. Chang, B.-H. Kuo, Y.-H. Wang, E.-C. Chen, F.-S. Shieu, Thickness dependence of the structural, electrical, and optical properties of amorphous indium zinc oxide thin films. *J. Alloy. Compd.* **743**, 603–609 (2018)
71. A. Mhamdi, B. Ouni, A. Amlouk, K. Boubaker, M. Amlouk, Study of nickel doping effects on structural, electrical and optical properties of sprayed ZnO semiconductor layers. *J. Alloy. Compd.* **582**, 810–822 (2014)
72. D.K. Schroder, *Semiconductor Material And Device Characterization* (Wiley, New York, 2006)
73. S. Baturay, A. Tombak, D. Kaya, Y.S. Ocak, M. Tokus, M. Aydemir, T. Kilicoglu, Modification of electrical and optical properties of CuO thin films by Ni doping. *J. Sol-Gel Sci. Technol.* **78**(2), 422–429 (2016)
74. J.S. Shaikh, R.C. Pawar, R.S. Devan, Y.R. Ma, P.P. Salvi, S.S. Kolekar, P.S. Patil, Synthesis and characterization of Ru doped CuO thin films for supercapacitor based on Bronsted acidic ionic liquid. *Electrochim. Acta* **56**(5), 2127–2134 (2011)
75. A. Ogwu, T. Darma, E. Bouquerel, Electrical resistivity of copper oxide thin films prepared by reactive magnetron sputtering. *J. Achiev Mater. Manuf. Eng.* **24**(1), 172–177 (2007)
76. Y. Shen, M. Guo, X. Xia, G. Shao, Role of materials chemistry on the electrical/electronic properties of CuO thin films. *Acta Mater.* **85**, 122–131 (2015)
77. R. Nitta, R. Taguchi, Y. Kubota, T. Kishi, A. Shishido, N. Matsushita, Novel bending sensor based on a solution-processed Cu<sub>2</sub>O film with high resolution covering a wide curvature range. *ACS Omega* **6**(48), 32647–32654 (2021)
78. Y. Sun, S.E. Thompson, T. Nishida, Physics of strain effects in semiconductors and metal-oxide-semiconductor field-effect transistors. *J. Appl. Phys.* **101**(10), 104503 (2007)
79. P. Kleimann, B. Semmache, M. Le Berre, D. Barbier, Stress-dependent hole effective masses and piezoresistive properties of p-type monocrystalline and polycrystalline silicon. *Phys. Rev. B* **57**(15), 8966–8971 (1998)
80. S. Dinç, B. Şahin, T. Kaya, Improved sensing response of nanostructured CuO thin films towards sweat rate monitoring: effect of Cr doping. *Mater. Sci. Semicond. Process.* **105**, 104698 (2020)
81. R. Bosigo, L.M. Lepodise, G. Chimowa, C. Muiva, Enhanced ethanol sensing response of nanostructured Ce-doped CuO thin films. *Mater. Chem. Phys.* **280**, 125841 (2022)

**Publisher's Note** Springer Nature remains neutral with regard to jurisdictional claims in published maps and institutional affiliations.

Springer Nature or its licensor holds exclusive rights to this article under a publishing agreement with the author(s) or other rightsholder(s); author self-archiving of the accepted manuscript version of this article is solely governed by the terms of such publishing agreement and applicable law.